LETTER

doi:10.1038/nature18928

Transfer of mitochondria from astrocytes to neurons after stroke

Kazuhide Hayakawa[1], Elga Esposito[1], Xiaohua Wang[1,2], Yasukazu Terasaki[1], Yi Liu[1,2], Changhong Xing[1], Xunming Ji[2] & Eng H. Lo[1]

Neurons can release damaged mitochondria and transfer them to astrocytes for disposal and recycling[1]. This ability to exchange mitochondria may represent a potential mode of cell-to-cell signalling in the central nervous system. Here we show that astrocytes in mice can also release functional mitochondria that enter neurons. Astrocytic release of extracellular mitochondrial particles was mediated by a calcium-dependent mechanism involving CD38 and cyclic ADP ribose signalling. Transient focal cerebral ischaemia in mice induced entry of astrocytic mitochondria into adjacent neurons, and this entry amplified cell survival signals. Suppression of CD38 signalling by short interfering RNA reduced extracellular mitochondria transfer and worsened neurological outcomes. These findings suggest a new mitochondrial mechanism of neuroglial crosstalk that may contribute to endogenous neuroprotective and neurorecovery mechanisms after stroke.

Astrocytes have broad roles in the central nervous system, and are involved in the regulation of neurodevelopment, neurotransmission, cerebral metabolism and blood flow[2–4]. Normal astrocytes protect neurons against oxidative stress and excitotoxicity[5–7]. By contrast, unhealthy astrocytes may release deleterious factors that damage neurons[8,9]. Healthy mitochondria may be essential for these neuroglial protective mechanisms because inhibition of astrocytic mitochondria makes neurons vulnerable to cell death[10]. Mitochondria comprise the intracellular cores for energetics and viability[11], but under some conditions mitochondria might also be released into the extracellular space[12]. For example, retinal neurons may transfer mitochondria to astrocytes for disposal and recycling[1], and bone-marrow-derived stromal cells may transfer mitochondria into pulmonary alveoli to suppress acute lung injury[13].

Here we investigated whether astrocytes can produce functional extracellular mitochondria to support neuronal viability after ischaemic stroke. Electron microscopy confirmed the presence of extracellular particles containing mitochondria in conditioned media from rat cortical astrocytes (Fig. 1a, Extended Data Fig. 1a). qNano analysis revealed that astrocyte-derived mitochondrial particles isolated by fluorescence-activated cell sorting (FACS) spanned a range of sizes from 300 to 1,100 nm (Extended Data Fig. 1b–d), and included populations that were positive for β1-integrin (79%) and CD63 (43%) (Extended Data Fig. 2). MitoTracker labelling suggested that these extracellular mitochondria may still be functional (Fig. 1b), and filtration of astrocyte-derived conditioned media through 0.2-μm filters depleted the amounts of functional mitochondria and reduced measurements of mitochondrial ATP, membrane potential and oxygen consumption (Fig. 1b–e).

An important question is whether extracellular mitochondria represent active signals or merely cellular debris. To address this, we investigated whether stimulated astrocytes could actively produce extracellular mitochondria. CD38 catalyses the synthesis of a calcium messenger, cyclic ADP-ribose (cADPR), in mitochondrial membranes[14,15]. In the brain, CD38 is mainly expressed in glial cells, and may have a role in neuroglial crosstalk since astrocytes increase CD38 expression in response to glutamate release from neurons[16]. On the basis of this background literature and the fact that most actively secreted cellular events involve calcium regulation, we decided to assess CD38–cADPR–calcium signalling as a candidate mechanism for the astrocytic production of extracellular mitochondria. First, we confirmed that rat cortical astrocytes expressed CD38 protein and contained CD38 or ADPR cyclase activity (Fig. 1f, g). We then used two methods to modify this pathway. When astrocytic CD38 was upregulated using CRISPR/Cas9 activation plasmids, the functional endpoints of extracellular mitochondria were significantly increased in conditioned media (Fig. 1h–k). When astrocytes were stimulated by cADPR to activate CD38 signalling, extracellular mitochondria were increased in conditioned media along with enhancement of functional endpoints in a calcium-dependent manner (Fig. 1l–n, Extended Data Fig. 3). Stimulation with cADPR did not appear to damage astrocyte viability (Fig. 1o), suggesting that this release of extracellular mitochondria was not due to nonspecific cytotoxicity.

If astrocytes can produce functional extracellular mitochondria, it is possible that these signals could affect adjacent neurons. When rat cortical neurons were subjected to oxygen–glucose deprivation, intracellular ATP levels fell and neuronal viability decreased, as expected (Fig. 2a–c, Extended Data Fig. 4a). When astrocyte-derived conditioned media containing extracellular mitochondrial particles was added to neurons, ATP levels increased and neuronal viability recovered (Fig. 2a–c, Extended Data Fig. 4a). However, when extracellular mitochondria were removed from the astrocyte-conditioned media, neuroprotection was no longer observed (Fig. 2a–c, Extended Data Fig. 4a). Similar results were obtained with immunostaining-based cell counts (Fig. 2d). As a control, ATP-liposomes were not significantly protective (Fig. 2e), suggesting that the entry of astrocytic mitochondria into neurons may generate additional benefits beyond ATP energetics per se. Fluorescent microscopy confirmed that astrocyte-derived mitochondria were present within treated neurons (Fig. 2f and Extended Data Fig. 4b).

Beyond the prevention of acute neuronal death, delayed neuroplasticity is also important for stroke outcomes. CD38 may be important for brain plasticity because CD38-deficient mice show worsened recovery after brain injury[17] and CD38 mutations may comprise risk factors for behavioural dysfunction[18]. Hence, we asked whether CD38-mediated astrocyte-to-neuron mitochondrial transfer may also influence neuroplasticity. Neurons were labelled with the green fluorescent protein (GFP)-containing construct CellLight Mitochondria-GFP and astrocytes were separately labelled with the red fluorescent probe MitoTracker Red CMXRos, and the two cell types were co-cultured together for 24 h. Confocal microscopy indicated that astrocyte-derived mitochondria were detected within soma and axon (Fig. 3a), and in these co-culture conditions, astrocytes supported neuronal survival after serum/glucose starvation in a CD38-dependent manner (Extended Data Fig. 5). When astrocytic mitochondria

[1]Neuroprotection Research Laboratory, Departments of Radiology and Neurology, Massachusetts General Hospital and Harvard Medical School, Charlestown, Massachusetts 02129, USA.
[2]Cerebrovascular Research Center, Xuanwu Hospital, Capital Medical University, Beijing 100053, China.

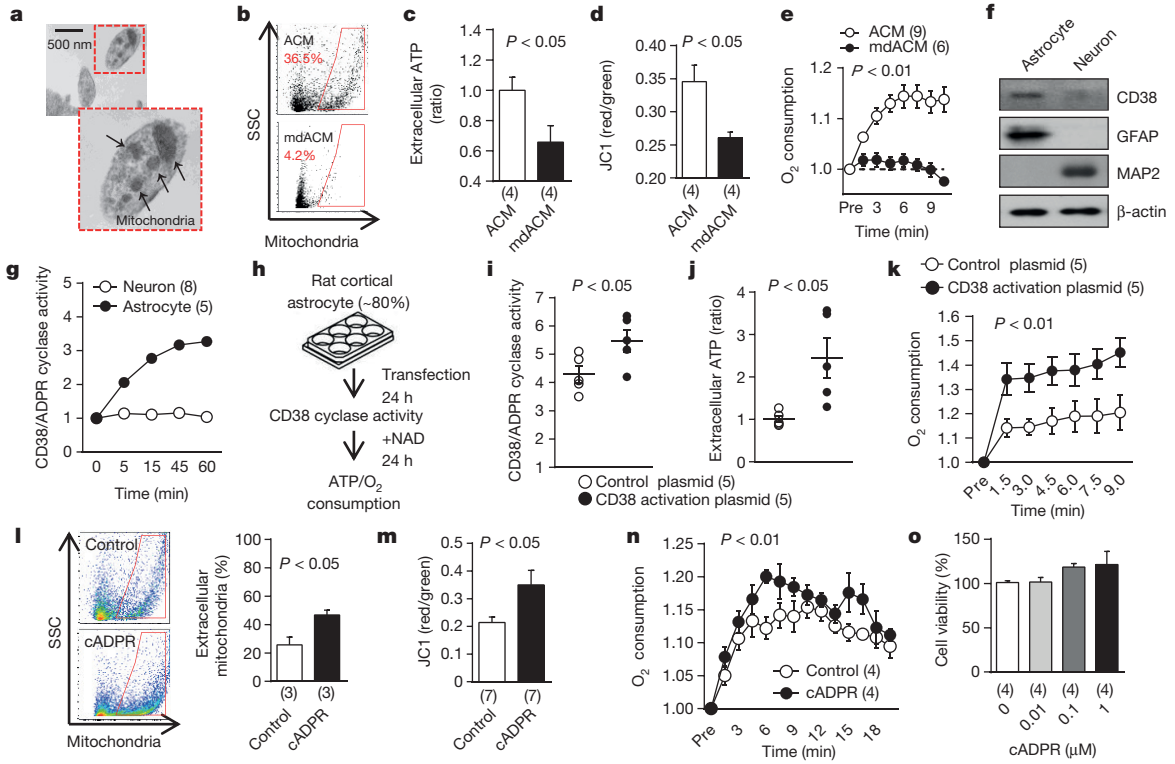

Figure 1 | Astrocytic CD38 and extracellular mitochondria. **a**, Transmission electron microscopy (TEM) of extracellular mitochondria in astrocyte-derived conditioned medium (ACM). Scale bar, 500 nm. **b**, Rat cortical astrocytes were labelled with MitoTracker Red CMXRos. FACS showed that filtration through 0.2-μm filters depleted levels of extracellular mitochondria in ACM (mitochondria-depleted ACM; mdACM). **c**–**e**, 0.2-μm filters reduced several markers of extracellular mitochondrial function in ACM: extracellular ATP (**c**, $n = 4$ independent experiments), membrane potential (JC1 ratio; **d**, $n = 4$ independent experiments), and oxygen consumption (**e**, $n = 3$ biological replicates, $n = 9$ or 6 independent experiments). **f**, Western blot confirmed higher CD38 levels in rat cortical astrocytes than in neurons. **g**, High and low levels of CD38 cyclase activity in astrocytes and neurons, respectively ($n = 2$ biological replicates, $n = 8$ or 5 independent experiments). **h**, Experimental schematic for testing CRISPR/Cas9-mediated CD38 activation. NAD, β-nicotinamide adenine dinucleotide sodium salt (200 μM). **i**, Twenty-four hours after transfection, CD38 cyclase activity was upregulated by CD38 activation plasmid ($n = 2$ biological replicates, $n = 5$ independent experiments). **j**, **k**, Extracellular ATP production (**j**) and oxygen consumption (**k**) were significantly increased by CD38 activation ($n = 2$ biological replicates, $n = 5$ independent experiments). **l**, FACS showed that extracellular mitochondria were increased by cADPR (1 μM) stimulation in astrocytes ($n = 3$ independent experiments). **m**, cADPR (1 μM) increased extracellular mitochondria membrane potential at 24 h ($n = 2$ biological replicates, $n = 7$ independent experiments). **n**, Oxygen consumption in extracellular mitochondria was increased by cADPR ($n = 2$ biological replicates, $n = 4$ independent experiments). **o**, cADPR did not cause astrocyte toxicity ($n = 2$ biological replicates, $n = 4$ independent experiments). Data are mean ± s.e.m. *P* values are from an unpaired *t*-test (**c**, **d**, **i**, **j**, **l**, **m**) or two-way analysis of variance (ANOVA) (**e**, **k**, **n**).

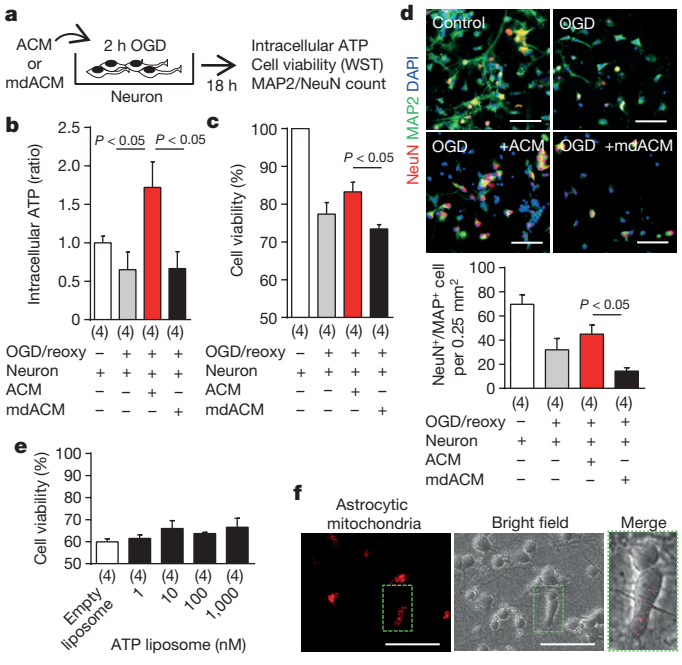

Figure 2 | Astrocytic extracellular mitochondria and neuroprotection. **a**, Experimental schematic to test neuroprotective effects of ACM or mdACM against oxygen–glucose deprivation (OGD) in rat cortical neurons. WST, water-soluble tetrazolium salt dye for cell viability assay. **b**, ACM but not mdACM rescued ATP levels in damaged neurons ($n = 2$ biological replicates, $n = 4$ independent experiments). **c**, ACM but not mdACM recovered neuronal viability after OGD ($n = 2$ biological replicates, $n = 4$ independent experiments). **d**, Immunostaining confirmed that neuroprotective effect of ACM but not mdACM ($n = 2$ biological replicates, $n = 4$ independent experiments). NeuN and MAP2 are neuronal markers. Scale bars, 100 μm. **e**, No statistically significant neuroprotection with liposomal ATP (1–1,000 nM) after OGD. **f**, Fluorescent microscopy suggests the presence of astrocyte mitochondria (labelled with MitoTracker Red CMXRos, 200 nM) within neurons. Scale bars, 100 μm. Data are mean ± s.e.m. *P* values are from a one-way ANOVA followed by Tukey's test.

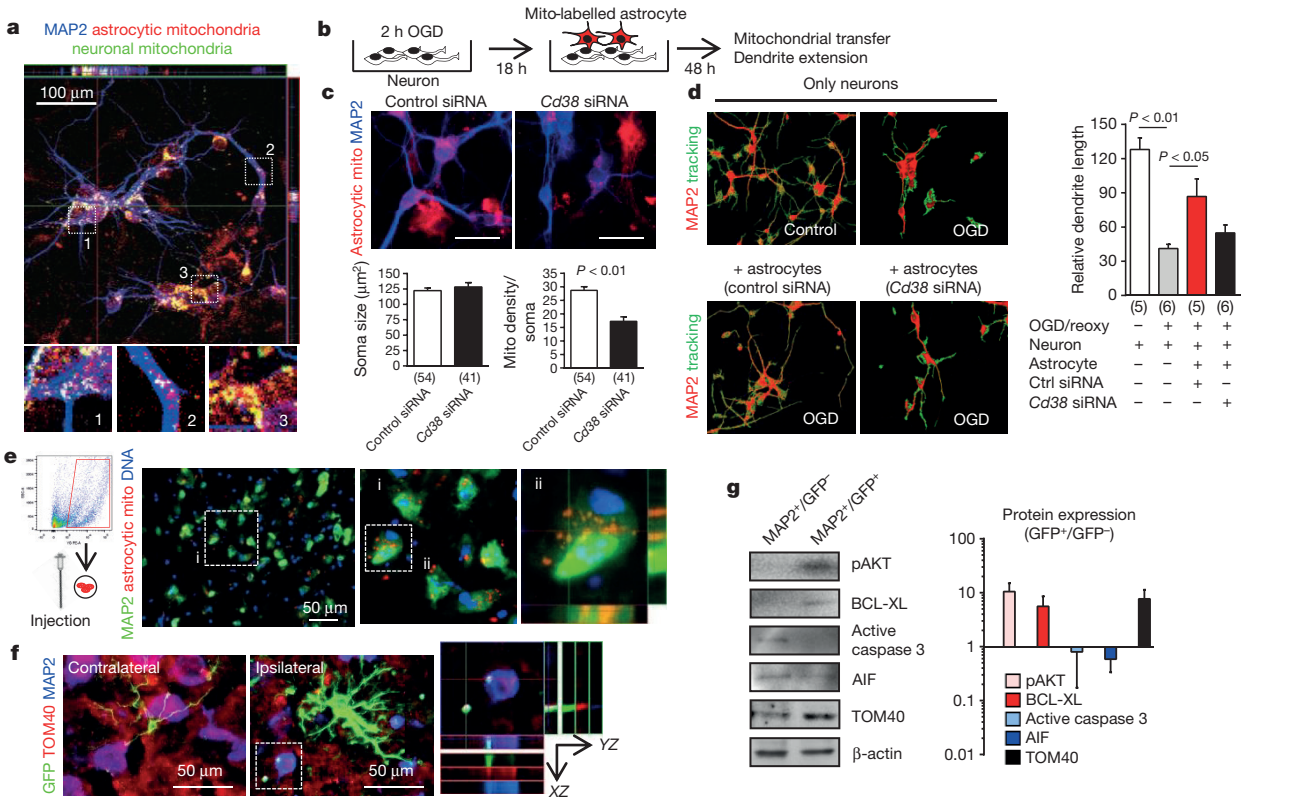

Figure 3 | Astrocytic mitochondria and neuroplasticity after ischaemic stress. a, Confocal microscopy revealed that astrocytic mitochondria (red, MitoTracker Red CMXRos) may be transferred into neural soma (1) and axon (2), and some may fuse with neuronal mitochondria (3; green, CellLight Mitochondria-GFP). **b**, Experimental schematic for co-culture studies. **c**, Soma size was unchanged but astrocytic mitochondrial density in neuronal soma was significantly decreased when CD38 was suppressed in astrocytes ($n = 54$ or 41 soma from $n = 2$ biological replicates, $n = 3$ independent experiments were counted). Scale bars, 20 µm. **d**, Quantification of dendrite elongation (MAP2 staining) ($n = 2$ biological replicates, $n = 5$ or 6 independent experiments). **e**, Male C57BL/6 J mice were subjected to 60 min transient focal ischaemia. Three days later, astrocyte mitochondrial particles (1,000 particles per 2 µl, MitoTracker Red CMXRos) were infused into cerebral cortex. Z-stack images showed transplanted astrocytic mitochondria (red) within peri-infarct neurons at 24 h. **f**, FVB/N-Tg (GFAPGFP)14Mes/J transgenic mice with fluorescently labelled astrocytes were subjected to 30 min transient focal ischaemia. Immunohistochemistry at 24 h suggested that GFP (GFAP)-positive particles co-stained with mitochondrial TOM40 were present in MAP2-positive neurons in peri-infarct cortex. **g**, Western blot indicated that GFP-positive neurons upregulated cell-survival-related proteins (phosphorylated-AKT, BCL-XL) but not apoptosis-related proteins (caspase 3, AIF) along with an increase in mitochondrial TOM40 ($n = 3$ mice). Isolated neurons expressed mature (neurofilament) but not neural stem-cell markers (nestin) (see Extended Data Fig. 7f). Data are mean ± s.e.m. *P* values are from an unpaired *t*-test (**c**) or one-way ANOVA followed by Tukey's test (**d**).

were made dysfunctional via inhibition of mitochondrial aconitase, cADPR-stimulated astrocytes no longer supported neuronal survival and axonal extension (Extended Data Fig. 6). To assess our hypothesis further, we asked whether this ability of astrocytes to transfer mitochondria could in fact enhance neuroplasticity under pathological conditions. Control or CD38-silenced astrocytes were co-cultured with surviving neurons after oxygen–glucose deprivation (Fig. 3b). Short interfering RNA (siRNA) suppression of CD38 in astrocytes reduced mitochondrial transfer (Fig. 3c) and dendrite regrowth after injury (Fig. 3d).

Taken together, these cellular findings appear consistent with the overall hypothesis that CD38 signalling may help astrocytes to transfer mitochondria into neurons and promote survival and plasticity after injury. But it is unclear whether this mechanism works *in vivo*. To address this question, we turned to a mouse model of focal cerebral ischaemia. First, primary mouse cortical astrocyte cultures were labelled with MitoTracker Red CMXRos and extracellular mitochondrial particles were collected. Mice were then subjected to focal cerebral ischaemia, and 3 days later, extracellular mitochondrial particles were directly injected into the peri-infarct cortex. After 24 h, immunostaining suggested that transplanted astrocytic mitochondria were present in neurons (Fig. 3e). Next, we turned to FVB/N-Tg (GFAPGFP)14Mes/J transgenic mice in which astrocytes are fluorescently labelled. When these mice were subjected to focal cerebral ischaemia, fluorescent mitochondrial particle signals appeared within adjacent neurons at 24 h after stroke (Fig. 3f). Neurons that were collected from ischaemic peri-infarct cortex via flow cytometry showed a general upregulation of cell-survival-related signals such as phosphorylated AKT and BCL-XL, along with an increase in the mitochondria marker TOM40 (Fig. 3g, Extended Data Fig. 7).

Finally, we attempted loss-of-function experiments to determine whether blocking CD38 signalling results in worsened outcomes after stroke. In our mouse model of focal cerebral ischaemia, CD38 was upregulated in the peri-infarct cortex (Extended Data Fig. 8a). At 5 days after stroke, *Cd38* siRNA or control siRNA was injected into cerebral ventricles (Fig. 4a). By 2 days after siRNA injections, total CD38 expression in the peri-infarct cortex was successfully downregulated (Extended Data Fig. 8b). There were no clear differences in infarct area or the total levels of GFAP-positive reactive astrocytes (Fig. 4b, c), but astrocyte subsets that expressed CD38 were significantly decreased without affecting the number of other CD38-expressing cells such as CD8 T cells and microglia/macrophages[19] (Fig. 4c, Extended Data Fig. 8c–g). To assess the levels of extracellular mitochondrial particles in this *in vivo* model, flow cytometry was used to analyse cerebrospinal fluid (CSF). GFAP-positive mitochondria were detected in CSF, and *Cd38* siRNA injections appeared to reduce

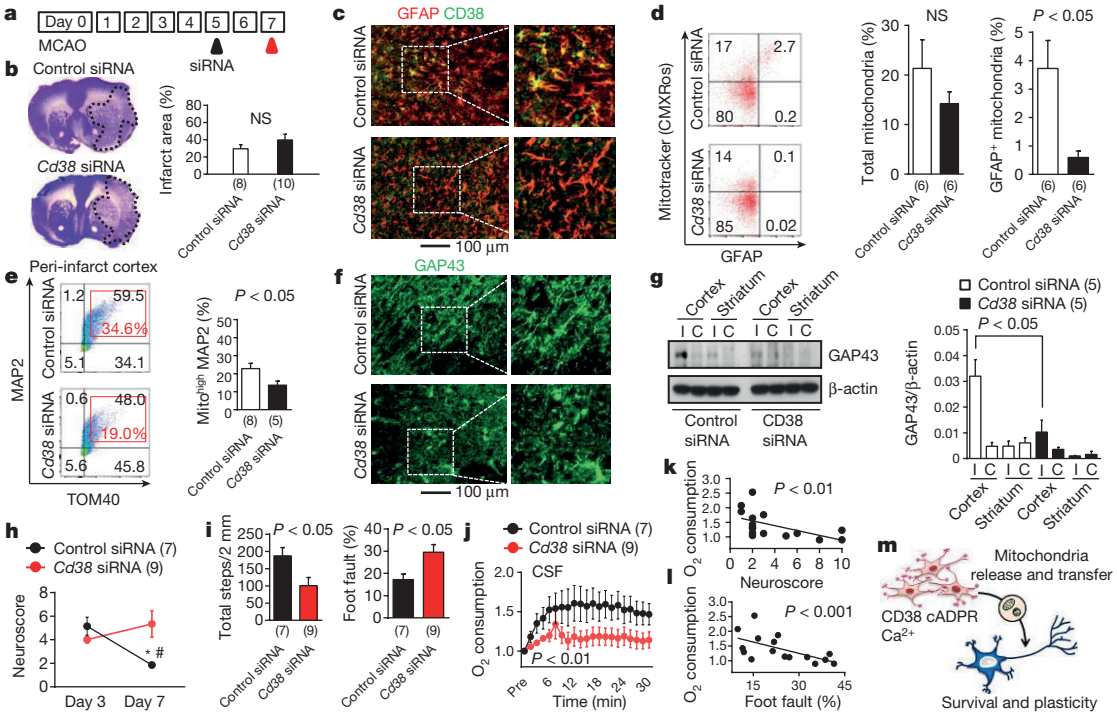

Figure 4 | Effects of *Cd38* siRNA on focal cerebral ischaemia. **a**, Male C57BL/6 J mice were subjected to transient 60 min focal ischaemia, and control or *Cd38* siRNA was injected into lateral ventricles 5 days after stroke. MCAO, middle cerebral artery occlusion. **b**, Nissl staining showed no difference in infarct size ($n = 8$ or 10 mice per group). NS, not significant. **c**, Immunostaining demonstrated that astrocytic CD38 was diminished by *Cd38* siRNA. **d**, Astrocytic CD38 suppression by siRNA reduced GFAP-positive mitochondria in CSF at 7 days ($n = 6$ mice per group). **e**, Neuronal mitochondria were decreased by *Cd38* siRNA ($n = 8$ or 5 mice per group). **f**, *Cd38* siRNA attenuated peri-infarct GAP43 immunostaining. **g**, Western blot confirmed a reduction of peri-infarct GAP43 protein within *Cd38*-siRNA-treated brains ($n = 5$ mice per group). C, contralateral hemisphere; I, ipsilateral hemisphere. **h**, **i**, Suppression of CD38 signalling worsened neurological outcomes in neurological severity scores (neuroscore) (**h**) and grid-walking test (**i**) ($n = 7$ or 9 mice per group). $^*P < 0.05$ versus day 3 control siRNA; $^\#P < 0.05$ versus day 7 *Cd38* siRNA. **j**, CD38 suppression decreased oxygen consumption in CSF mitochondria ($n = 7$ or 9 mice per group). **k**, **l**, Mitochondrial function in CSF was negatively correlated with neurological outcomes. Data are mean ± s.e.m. *P* values are from an unpaired *t*-test (**b**, **d**, **e**, **i**), one-way ANOVA followed by Tukey's test (**g**), repeated-measures two-way ANOVA followed by Bonferroni test (**h**), two-way ANOVA (**j**), or Spearman's rank correlation (**k**, **l**). **m**, Schematic of CD38 regulation of mitochondria release/transfer hypothesis between astrocytes and neurons.

this extracellular population of astrocyte-derived mitochondria (Fig. 4d). At the same time, flow cytometry was used to quantify levels of MAP2 neuronal mitochondria (Extended Data Fig. 9). Brains treated with *Cd38* siRNA showed a significant reduction in neuronal mitochondria (Fig. 4e), suggesting that interfering with CD38 signalling may have suppressed endogenous astrocyte-to-neuron mitochondrial transfer. These effects were accompanied by a reduction in peri-infarct GAP43 (a surrogate marker of neuroplasticity; Fig. 4f, g) as well as worsened neurological outcomes (Fig. 4h, i). Furthermore, CD38 suppression significantly decreased oxygen consumption measurements in CSF-derived extracellular mitochondrial particles (Fig. 4j), and neurological outcomes seemed to be negatively correlated with these functional endpoints (Fig. 4k, l), suggesting that CSF mitochondrial function may be a potential biomarker of neuroglial signalling after stroke.

Taken together, these findings suggest that astrocytes may release extracellular mitochondrial particles via CD38-mediated mechanisms that enter neurons after stroke (Fig. 4m). However, there are a few caveats and the detailed mechanisms and generalizability of these proof-of-concept findings should warrant further investigation. First, the dynamics of extracellular mitochondria release and entry into neurons as well as quantitative thresholds for functional benefit remain to be fully defined (Extended Data Fig. 10a–i). A second caveat relates to mitochondrial entry mechanisms. In neurons, endocytosis may be regulated by dynamin/clathrin[20] or integrin pathways[21]. In our models, integrin-mediated Src/Syk signalling may be involved (Extended Data Fig. 10j–m). How integrin-mediated mitochondrial transfer is modulated under different disease conditions requires further study. Third, CD38 is also expressed in immune cells. In this study, CD38 suppression by siRNA *in vivo* did not appear to affect T cells or microglia/macrophages, but the balance between potentially beneficial CD38 signals in astrocytes versus deleterious CD38 signals in immune cells should be carefully considered. A fourth caveat is whether other glial cells may participate. Microglia, oligodendrocytes and pericytes are activated after stroke[22,23], so their potential roles in mitochondrial exchange warrant further investigation. Finally, astrocytes can produce many factors for protecting and restoring neurons, including tPA, high-mobility group box 1 (HMGB1), extracellular microvesicles containing VEGF and FGF-2, and various microRNAs[24–27]. How mitochondrial particles may interact with these other extracellular signals should be explored.

Non-cell autonomous signalling is vital for central nervous system recovery after injury or disease[28,29]. In the context of cerebral ischaemia, the present study suggests that astrocytes may release extracellular mitochondrial particles that enter neurons to support cell viability and recovery after stroke.

Online Content Methods, along with any additional Extended Data display items and Source Data, are available in the online version of the paper; references unique to these sections appear only in the online paper.

Received 11 January; accepted 14 June 2016.

1. Davis, C. H. *et al.* Transcellular degradation of axonal mitochondria. *Proc. Natl Acad. Sci. USA* **111,** 9633–9638 (2014).
2. Iadecola, C. & Nedergaard, M. Glial regulation of the cerebral microvasculature. *Nat. Neurosci.* **10,** 1369–1376 (2007).
3. Attwell, D. *et al.* Glial and neuronal control of brain blood flow. *Nature* **468,** 232–243 (2010).

4. Khakh, B. S. & Sofroniew, M. V. Diversity of astrocyte functions and phenotypes in neural circuits. *Nat. Neurosci.* **18,** 942–952 (2015).
5. Rosenberg, P. A. & Aizenman, E. Hundred-fold increase in neuronal vulnerability to glutamate toxicity in astrocyte-poor cultures of rat cerebral cortex. *Neurosci. Lett.* **103,** 162–168 (1989).
6. Wang, X. F. & Cynader, M. S. Pyruvate released by astrocytes protects neurons from copper-catalyzed cysteine neurotoxicity. *J. Neurosci.* **21,** 3322–3331 (2001).
7. Ouyang, Y. B. *et al.* Astrocyte-enriched miR-29a targets PUMA and reduces neuronal vulnerability to forebrain ischemia. *Glia* **61,** 1784–1794 (2013).
8. Nagai, M. *et al.* Astrocytes expressing ALS-linked mutated SOD1 release factors selectively toxic to motor neurons. *Nat. Neurosci.* **10,** 615–622 (2007).
9. Haidet-Phillips, A. M. *et al.* Astrocytes from familial and sporadic ALS patients are toxic to motor neurons. *Nat. Biotechnol.* **29,** 824–828 (2011).
10. Voloboueva, L. A., Suh, S. W., Swanson, R. A. & Giffard, R. G. Inhibition of mitochondrial function in astrocytes: implications for neuroprotection. *J. Neurochem.* **102,** 1383–1394 (2007).
11. Anne Stetler, R., Leak, R. K., Gao, Y. & Chen, J. The dynamics of the mitochondrial organelle as a potential therapeutic target. *J. Cereb. Blood Flow Metab.* **33,** 22–32 (2013).
12. Falchi, A. M. *et al.* Astrocytes shed large membrane vesicles that contain mitochondria, lipid droplets and ATP. *Histochem. Cell Biol.* **139,** 221–231 (2013).
13. Islam, M. N. *et al.* Mitochondrial transfer from bone-marrow-derived stromal cells to pulmonary alveoli protects against acute lung injury. *Nat. Med.* **18,** 759–765 (2012).
14. Aksoy, P., White, T. A., Thompson, M. & Chini, E. N. Regulation of intracellular levels of NAD: a novel role for CD38. *Biochem. Biophys. Res. Commun.* **345,** 1386–1392 (2006).
15. Guse, A. H. & Lee, H. C. NAADP: a universal Ca^{2+} trigger. *Sci. Signal.* **1,** re10 (2008).
16. Bruzzone, S. *et al.* Glutamate-mediated overexpression of CD38 in astrocytes cultured with neurones. *J. Neurochem.* **89,** 264–272 (2004).
17. Levy, A. *et al.* CD38 facilitates recovery from traumatic brain injury. *J. Neurotrauma* **26,** 1521–1533 (2009).
18. Higashida, H. *et al.* Social memory, amnesia, and autism: brain oxytocin secretion is regulated by NAD+ metabolites and single nucleotide polymorphisms of CD38. *Neurochem. Int.* **61,** 828–838 (2012).
19. Choe, C. U. *et al.* CD38 exacerbates focal cytokine production, postischemic inflammation and brain injury after focal cerebral ischemia. *PLoS One* **6,** e19046 (2011).
20. Frühbeis, C. *et al.* Neurotransmitter-triggered transfer of exosomes mediates oligodendrocyte-neuron communication. *PLoS Biol.* **11,** e1001604 (2013).
21. Bowen, S. *et al.* The phagocytic capacity of neurones. *Eur. J. Neurosci.* **25,** 2947–2955 (2007).
22. Winkler, E. A., Bell, R. D. & Zlokovic, B. V. Central nervous system pericytes in health and disease. *Nat. Neurosci.* **14,** 1398–1405 (2011).
23. Hu, X. *et al.* Microglial and macrophage polarization—new prospects for brain repair. *Nat. Rev. Neurol.* **11,** 56–64 (2015).
24. Xin, H. *et al.* Increasing tPA activity in astrocytes induced by multipotent mesenchymal stromal cells facilitate neurite outgrowth after stroke in the mouse. *PLoS One* **5,** e9027 (2010).
25. Hayakawa, K., Pham, L. D., Katusic, Z. S., Arai, K. & Lo, E. H. Astrocytic high-mobility group box 1 promotes endothelial progenitor cell-mediated neurovascular remodeling during stroke recovery. *Proc. Natl Acad. Sci. USA* **109,** 7505–7510 (2012).
26. Proia, P. *et al.* Astrocytes shed extracellular vesicles that contain fibroblast growth factor-2 and vascular endothelial growth factor. *Int. J. Mol. Med.* **21,** 63–67 (2008).
27. Li, Y., Liu, Z., Xin, H. & Chopp, M. The role of astrocytes in mediating exogenous cell-based restorative therapy for stroke. *Glia* **62,** 1–16 (2014).
28. Lo, E. H. Degeneration and repair in central nervous system disease. *Nat. Med.* **16,** 1205–1209 (2010).
29. Xing, C. & Lo, E. H. Help-me signaling: Non-cell autonomous mechanisms of neuroprotection and neurorecovery. *Prog. Neurobiol.* http://dx.doi.org/10.1016/j.pneurobio.2016.04.004 (2016).

Acknowledgements This work was supported in part by grants from the National Institutes of Health (NIH), the Rappaport Foundation, and the China National Natural Science Foundation Award For Distinguished Young Scholars. Electron microscopy was performed in the Center for Systems Biology. Cytometric assessments were supported by the Department of Pathology Flow and Image Cytometry Core. The authors thank J. Felton and J. Zwicker for assistance with qNano analysis.

Author Contributions K.H. contributed to manuscript preparation, hypothesis generation, experimental design/analysis and conducted experiments. E.E., X.W., Y.T., Y.L. and C.X. conducted experiments and helped with data analysis. X.J. and E.H.L. contributed to manuscript preparation, hypothesis generation and experimental design.

Author Information Reprints and permissions information is available at www.nature.com/reprints. The authors declare no competing financial interests. Readers are welcome to comment on the online version of the paper. Correspondence and requests for materials should be addressed to K.H. (khayakawa1@mgh.harvard.edu), X.J. (jixunming@vip.163.com) or E.H.L. (Lo@helix.mgh.harvard.edu).

METHODS

No statistical methods were used to predetermine sample size.

Reagents. BAPTA-AM (A1076), cADPR (C7344), β-nicotinamide adenine dinucleotide sodium salt (N0632) and dynasore hydrate (D7693) were purchased from Sigma, and RGDS peptide (3498) and MNS (2877/50) were from R&D systems.

Mouse focal cerebral ischaemia model. All experiments were performed following an institutionally approved protocol in accordance with National Institutes of Health guidelines and with the United States Public Health Service's Policy on Human Care and Use of Laboratory Animals. Our methods also included randomization, blinding and statistical criteria consistent with ARRIVE guidelines (Animals in Research: Reporting *In vivo* Experiments). In brief, male C57BL/6 J (12–14 weeks) or FVB/N-Tg (GFAPGFP)14Mes/J mice are anaesthetized with 5% to 1% isoflurane, and rectal temperatures and cerebral blood flow are monitored. After midline skin incision, 7-0 nylon monofilament coated with silicon resin was introduced through a small incision into the common carotid artery. Adequate cerebral ischaemia was assessed by Laser Doppler flowmetry and by examining forelimb flexion after the mice recovered from anaesthesia. The mice were reanaesthetized, and reperfusion was established by withdrawal of the filament. Functional outcome after stroke was assessed by neurological severity scores and the foot-fault test[25].

Primary neuron cultures. Primary neuron cultures were prepared from cerebral cortices of embryonic day (E)17 Sprague–Dawley rat embryos or E17 FVB/N-Tg (GFAPGFP)14Mes/J mouse embryos. In brief, cortices were dissected and dissociated using papain dissociation system (Worthington Biochemical Corporation, LK003150). Cells were spread on plates coated with poly-D-lysine (Sigma, P7886) and cultured in DMEM (NBM, Life Technology, 11965-084) containing 25 mM glucose, 4 mM glutamine, 1 mM sodium pyruvate, and 5% FBS at a density of 2×10^5 cells ml^{-1} (1 ml for 12-well format, 0.5 ml for 24-well format). At 24 h after seeding, the medium was changed to Neurobasal medium (Invitrogen, 21103-049) supplemented with B-27 (Invitrogen, 17504044) and 0.5 mM glutamine. Cells were cultured at 37 °C in a humidified chamber of 95% air and 5% CO_2. Cultures were used for experiments from 7 to 10 days after seeding.

Primary astrocyte cultures. Primary astrocyte cultures were prepared from cerebral cortices of 2-day-old neonatal Sprague–Dawley rats or E17 C57BL/6 J mice. In brief, dissociated cortical cells were suspended in DMEM (Life Technology, 11965-084) containing 25 mM glucose, 4 mM glutamine, 1 mM sodium pyruvate, and 10% FBS and plated on uncoated 25 cm^2 flasks at a density of 6×10^5 cells cm^{-2}. Monolayers of type 1 astrocytes were obtained 12–14 days after plating. Non-astrocytic cells such as microglia and neurons were detached from the flasks by shaking and removed by changing the medium. Astrocytes were dissociated by trypsinization and then reseeded on uncoated T75 flasks. After the cells reached 70–80% confluence, cultures were switched to Neurobasal medium containing 1% penicillin/streptomycin or DMEM containing 1% penicillin/streptomycin, and astrocyte-conditioned media (ACM) were collected 24 h later. Collected ACM was treated by spin cell debris down with centrifuging at 2,000*g* for 10 min or by filtrating through a 1.2-μm syringe filter for further experiments.

OGD and reoxygenation. OGD experiments were performed using a specialized, humidified chamber (Heidolph, incubator 1000, Brinkmann Instruments) kept at 37 °C, which contained an anaerobic gas mixture (90% N_2, 5% H_2, and 5% CO_2). To initiate OGD, culture medium was replaced with deoxygenated, glucose-free DMEM (Life Technology, 11966-025). After 2 h challenge, cultures were removed from the anaerobic chamber, and the OGD solution in the cultures was replaced with maintenance medium. Cells were then allowed to recover for 18 h (for neurotoxicity assay) and 72 h (for siRNA/astrocyte coculture) in a regular incubator.

Cell viability assays. Neuronal injury was measured by standard cell cytotoxicity assays such as lactate dehydrogenase (LDH) using the Cytotoxicity Detection Kit (Roche Applied Science, 11644793001) and/or Cell Counting Kit 8 cytotoxicity assay (DOJINDO, CK04-13). For the LDH assay, 100% cell death was induced with 0.5% Triton X-100 in sister culture. The relative assessments of neuronal injury were normalized by comparison with 100% cell death (LDH assay) or with control cell as 100% cell survival (CCK8).

Determination of CD38/ADPR-cyclase activity. ADPR cyclase activity was determined fluorometrically using nicotinamide guanine dinucleotide (NGD^+) (Sigma, N5131) as a substrate as described previously[30,31]. Astrocytes or neurons were incubated with 200 μM NGD^+, and the production of cGDPR was determined at excitation/emission wavelengths of Ex 300 nm/Em 410 nm with a microplate reader.

ATP measurement. Intracellular or extracellular ATP was determined by CellTiter-Glo luminescence kit (Promega, G7570), which can perform cell lysis and generate a luminescent signal proportional to the amount of ATP present. In brief, opaque-walled 96-well plates with culture media (50 μl) or cell lysate (50 μl) were prepared. CellTiter-Glo luminescence test solution (50 μl) was added and incubated for 30 min at room temperature. Luminescent signal was determined by luminescence microplate reader.

Liposomal ATP treatment. Liposomal ATP was obtained from Encapsula NanoScience. In brief, we used lyophilized proliposomes compose of 7:3 molar ratio of L-α-phosphatidylcholine: L-α-phosphatidylserine containing ATP which forms 100 nm liposomal ATP upon hydration. ATP-loaded liposome (1–1,000 nM) was co-incubated with neurons following OGD, and cell viability was analysed after 18 h reoxygenation.

Mitochondria membrane potential measurement. To monitor mitochondrial health, JC-1 dye (Invitrogen, T-3168) was used to assess mitochondrial membrane potential. Rat cortical astrocytes or media were incubated with JC1 (5 μM or 1 μM) for 30 min at 37 °C. JC1 dye exhibits potential-dependent accumulation in mitochondria, indicated by fluorescence emission shift from green (Ex 485 nm/Em 516 nm) to red (Ex 579 nm/Em 599 nm). Mitochondria membrane potential was determined by the fluorescent ratio with a fluorescent microplate reader.

Oxygen consumption analysis. Real-time oxygen consumption in astrocytic particles or in CSF samples was measured by the Mito-ID Extracellular O2 sensor kit (Enzo Life Science, ENZ-51045) according to the instruction provided Enzo Life Science. In brief, astrocytes (70–80% confluent cells per well per 100 μl) or particle fractions (100 μl; 25-fold concentrated astrocytic conditioned media) were prepared in non-coated regular 96 wells, and O_2 sensor probe (10 μl) was added into each well. Each CSF sample (8–20 μl) was collected from cisterna magna at day 7 after focal cerebral ischaemia. After centrifugation at 2,000*g* for 10 min, 6 μl CSF was diluted in 54 μl PBS, and 6 μl O_2 sensor probe was added into each well. After covering with 100 μl (50 μl for CSF sample) of Mito-ID HS Oil, the plates were read with filter combination of 340 nm for excitation and 642 nm of emission at 30 °C.

Electron microscopy analysis. Rat cortical astrocytes or pellets from astrocyte-conditioned media were fixed in 2.0% glutaraldehyde in 0.1 M sodium cacodylate buffer, pH 7.4 (Electron Microscopy Sciences) for 1 h at room temperature on a rocker. They were rinsed in cacodylate buffer, gently scraped and pelleted and post-fixed in 1.0% osmium tetroxide in cacodylate buffer for 1 h on ice. They were rinsed in buffer and stabilized with a small amount of 2% agarose in PBS to hold them together. They were then dehydrated through a graded series of ethanol to 100%, followed by propylene oxide, 100%. They were infiltrated with Epon resin (Ted Pella) in a 1:1 solution of Epon:propylene oxide overnight on a rocker at room temperature. The next day they were placed in fresh Epon for several hours and then embedded in Epon overnight at 60 °C. Thin sections were cut on a Leica EM UC7 ultramicrotome, collected on formvar-coated grids, stained with uranyl acetate and lead citrate and examined in a JEOL JEM 1011 transmission electron microscope at 80 kV. Images were collected using an AMT digital imaging system (Advanced Microscopy Techniques). These methods are similar to previous descriptions of extracellular particle and mitochondria detection in astrocyte cultures[12].

FACS analysis. Standard FACS analysis was performed by BD LSR II or BD Fortessa as described previously[25,32,33]. ACM was collected from rat cortical astrocytes labelled with MitoTracker Red CMXRos followed by filtrating through a 1.2-μm syringe filter. The supernatant was used to sort labelled mitochondria fraction by FACSAriaII cell sorter configured with 561 nm air cooled laser. Brain cells were collected from peri-infarct cortex after stroke. In brief, tissues are gently minced and then digested at 37 °C for 30 min with an enzyme cocktail (collagenase type I, DNase I, Sigma Aldrich). CSF samples were prepared for further staining after centrifugation at 2,000*g* for 10 min. FACS analysis was performed using an unstained or phenotype control for determining appropriate gates, voltages, and compensations required in multivariate flow cytometry.

Measurement of particle size. Particle size following extracellular mitochondria isolation by FACS was determined by qNano (iZON). Nanopore-based detection allows particle-by-particle assessment of complex mixtures. Optimization of pore size to particle size, by adjusting the stretch of the pore, allows highly accurate measurement[34]. Particles containing mitochondria were sorted using FACS analysis, then particle sizes were quantified by NP400 and using CPC400 calibration particle.

Western blot analysis. Western blot was performed as previously reported[25]. ProPREP Protein Extraction Solution (iNtRON Biotechnology, 17081) or Qproteome FFPE Tissue kit (Qiagen, 37623) was used to collect samples. Each sample was loaded onto 4–20% Tris-glycine gels. After electrophoresis and transferring to nitrocellulose membranes, the membranes were blocked in Tris-buffered saline containing 0.1% Tween 20 and 0.2% I-block (Tropix, T2015) for 90 min at room temperature. Membranes were then incubated overnight at 4 °C with the following primary antibodies, anti-β-actin (1:1,000, Sigma-Aldrich, A5441), anti-GFAP antibody (1:1,000, BD Biosciences, 556328), anti-MAP2 antibody (1:500, Abcam, ab11267 or ab32454), anti-CD38 antibody (1:500, Santacruz, sc-7049), anti-TOM40 (1:200, Santacruz, sc-11414), anti-phosphorylated AKT (1:500, Cell Signaling, 9271), anti-BCL-XL (1:500, Cell Signaling, 2764), anti-active caspase 3

(1:200, Abcam, ab32042), anti-AIF (1:500, Abcam, ab32516), and anti-GAP43 (1:500, Santacruz, sc-17790). After incubation with peroxidase-conjugated secondary antibodies, visualization was enhanced by chemiluminescence (GE Healthcare, NA931 (anti-mouse), NA934 (anti-rabbit), or NA935 (anti-rat)). Optical density was assessed using the NIH Image analysis software.

Immunocytochemistry and immunohistochemistry. Immunocytochemistry and immunohistochemistry were performed as described previously[35,36]. After staining with primary antibody and fluorescent-tagged secondary antibody, nuclei were counterstained with or without 4,6-diamidino-2-phenylindole (DAPI), and coverslips were placed. Immunostaining images or time lapse images were obtained with a fluorescence microscope (Nikon ECLIPSE Ti-S) interfaced with a digital charge-coupled device camera and an image analysis system or confocal microscope analysis using Carl Zeiss Laser Scanning Confocal Microscope Pascal 5 LSM and Pascal 5 LSM software Version 3.2. Dendrite elongation was assessed following MAP2 staining followed by NeuriteQuant analysis[37].

CRISPR activation plasmid transfection. Control CRISPR activation plasmid (sc-437275), and rat CD38 CRISPR activation plasmid (sc-437321-ACT) were obtained from Santa Cruz Biotechnology. Transfection was performed according to the transfection protocol for cell cultures from Santa Cruz Biotechnology. In brief, 1 ml of plasmid transfection reagent mixture (transfection reagent, sc-395739, transfection medium, sc-108062) was co-incubated with astrocytes for 24 h in a 5% CO_2 incubator at 37 °C, and then CD38 cyclase activity was assessed to confirm efficiency of transfection.

siRNA experiments. Control siRNA and *Cd38* siRNA were obtained from Santa Cruz Biotechnology. Control siRNA (sc-37007) consists of a scrambled sequence that will not lead to the specific degradation of any known cellular mRNA. Mouse *Cd38* siRNA (sc-37246) or rat *Cd38* siRNA (sc-270394) is each pool of 3 target-specific 19–25-nucleotide siRNAs designed to knock down gene expression. The sequences for mouse *Cd38* siRNAs are: 5′-GUGUACUACCAACAUUCAA-3′, 5′-GUGUGUCUUUAGUAGGUAU-3′, 5′-CCAGUUUGUGAUUGUUGA-3′. Rat *Cd38* siRNAs are: sequence 1: 5′-CUCAAACCAUACCAUGUAA-3′, sequence 2: 5′-GGAAGAGCUUCCCAAUACA-3′, sequence 3: 5′-GUGUUAU CGUCUAGCAAUA-3′.

siRNA was prepared according to the transfection protocol for cell cultures from Santa Cruz Biotechnology. In brief, 1 ml of siRNA transfection reagent mixture (transfection reagent, sc-29528, transfection medium, sc-36868) was co-incubated with astrocytes for 6 h in a 5% CO_2 incubator at 37 °C, and then the same amount of DMEM 20% FBS was added. An additional incubation was performed for 18 h.

Statistical analysis. Results were expressed as mean ± s.e.m. When only two groups were compared, an unpaired *t*-test was used. Multiple comparisons were evaluated by one-way ANOVA followed by Tukey's test, two-way ANOVA or repeated-measure two-way ANOVA followed by Bonferroni test. Correlation was evaluated by Spearman's rank correlation. $P < 0.05$ was considered statistically significant. Statistical analyses were performed using GraphPad Prism 6.

30. Rah, S. Y., Park, K. H., Han, M. K., Im, M. J. & Kim, U. H. Activation of CD38 by interleukin-8 signaling regulates intracellular Ca^{2+} level and motility of lymphokine-activated killer cells. *J. Biol. Chem.* **280,** 2888–2895 (2005).
31. Graeff, R. M., Walseth, T. F., Fryxell, K., Branton, W. D. & Lee, H. C. Enzymatic synthesis and characterizations of cyclic GDP-ribose. A procedure for distinguishing enzymes with ADP-ribosyl cyclase activity. *J. Biol. Chem.* **269,** 30260–30267 (1994).
32. Bi, B. *et al.* Cortical glial fibrillary acidic protein-positive cells generate neurons after perinatal hypoxic injury. *J. Neurosci.* **31,** 9205–9221 (2011).
33. Cruz, F. C. *et al.* New technologies for examining the role of neuronal ensembles in drug addiction and fear. *Nat. Rev. Neurosci.* **14,** 743–754 (2013).
34. Vogel, R. *et al.* Quantitative sizing of nano/microparticles with a tunable elastomeric pore sensor. *Anal. Chem.* **83,** 3499–3506 (2011).
35. Hayakawa, K. *et al.* Inhibition of reactive astrocytes with fluorocitrate retards neurovascular remodeling and recovery after focal cerebral ischemia in mice. *J. Cereb. Blood Flow Metab.* **30,** 871–882 (2010).
36. Hayakawa, K., Arai, K. & Lo, E. H. Role of ERK map kinase and CRM1 in IL-1β-stimulated release of HMGB1 from cortical astrocytes. *Glia* **58,** 1007–1015 (2010).
37. Dehmelt, L., Poplawski, G., Hwang, E. & Halpain, S. NeuriteQuant: an open source toolkit for high content screens of neuronal morphogenesis. *BMC Neurosci.* **12,** 100 (2011).

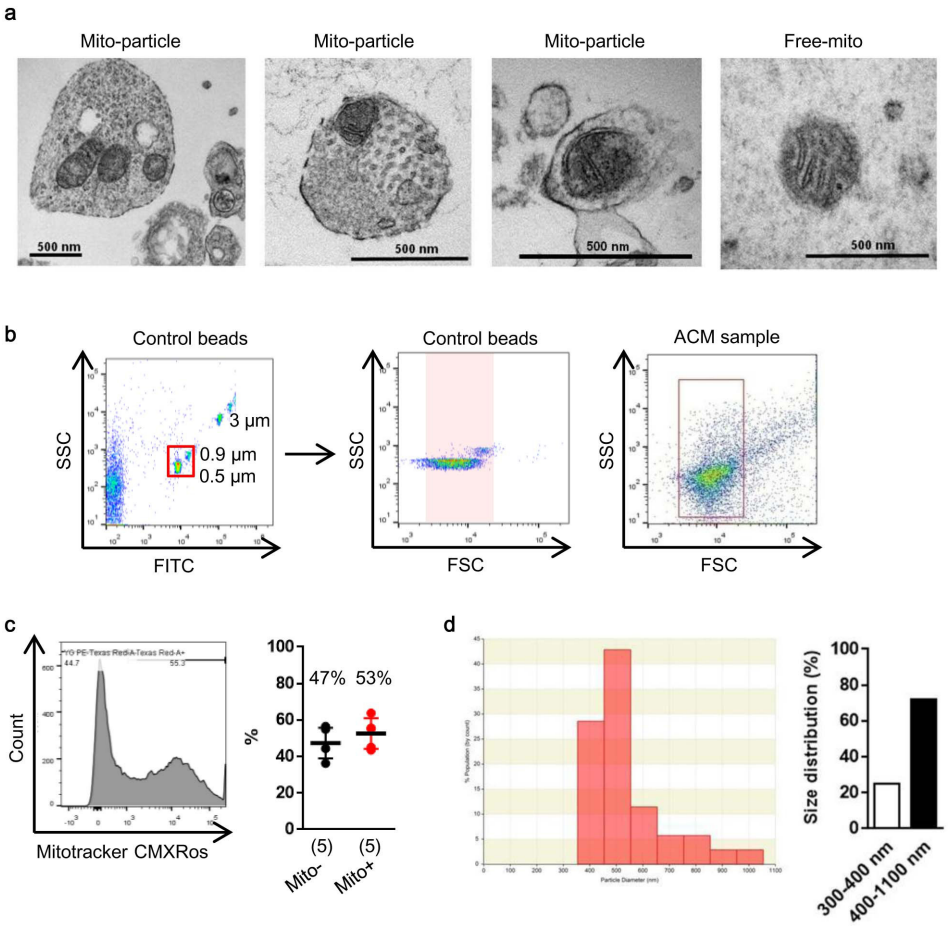

Extended Data Figure 1 | Astrocytic mitochondria particle detection. **a**, Electron microscopic analysis demonstrated that mitochondria were detected within extracellular astrocyte-derived particles. Free mitochondria were also found in ACM. **b**, In FACS analysis, control beads were used to gate populations ranging in size from 500 to 900 nm. **c**, In ACM, approximately 53% of particles in the size range were positive for functional mitochondria ($n = 2$ biological replicates, $n = 5$ independent experiments). **d**, After FACS analysis to isolate the extracellular mitochondria fraction from ACM, particle size was measured by qNano analysis. Consistent with electron microscopy analysis, a range of size distributions was observed (~25%: 300–400 nm, ~75%: 400–1,100 nm). Data are mean ± s.e.m.

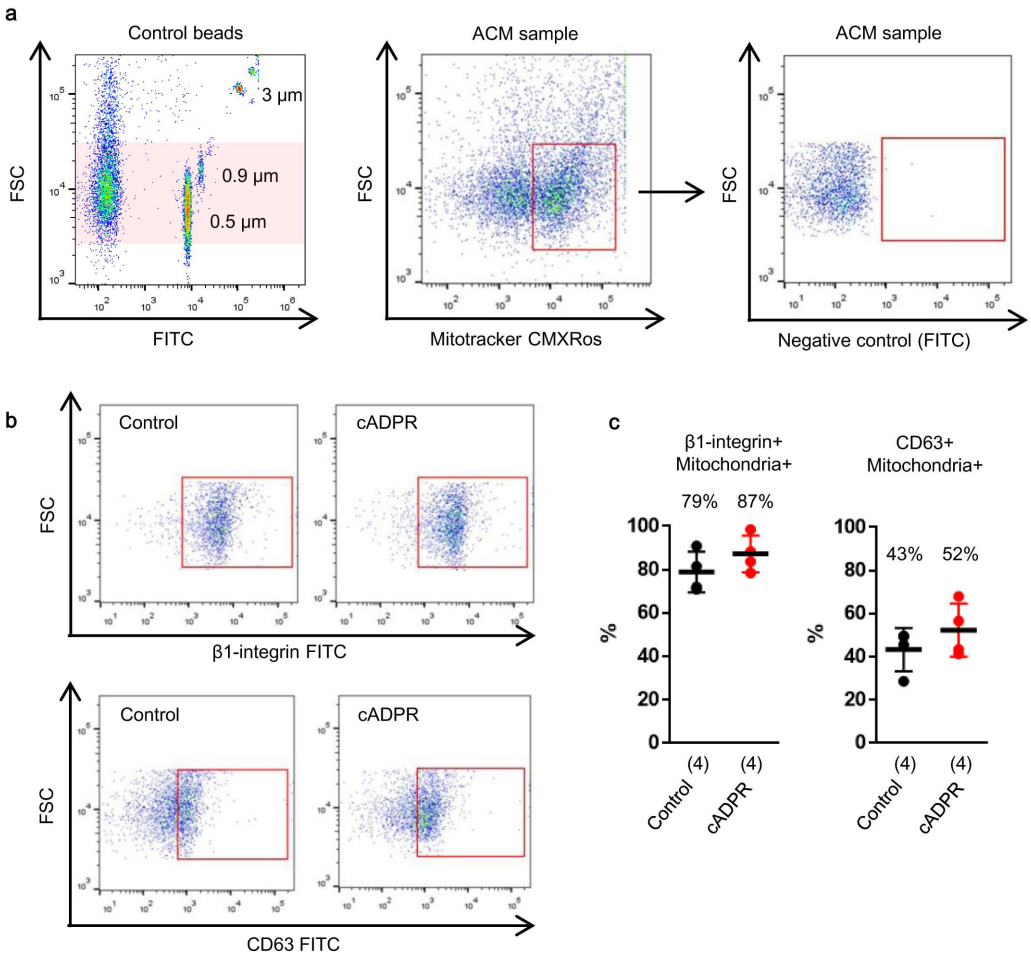

Extended Data Figure 2 | Characteristics of astrocytic mitochondrial particles in FACS analysis. a, Mitochondrial particles were identified by FACS. **b**, Of these mitochondrial particles, FACS analysis showed that approximately 79% and 43% of particles express β1-integrin and CD63, respectively ($n = 2$ biological replicates, $n = 4$ independent experiments). cADPR (1 µM) did not appear to affect these distributions ($n = 2$ biological replicates, $n = 4$ independent experiments). Data are mean ± s.e.m.

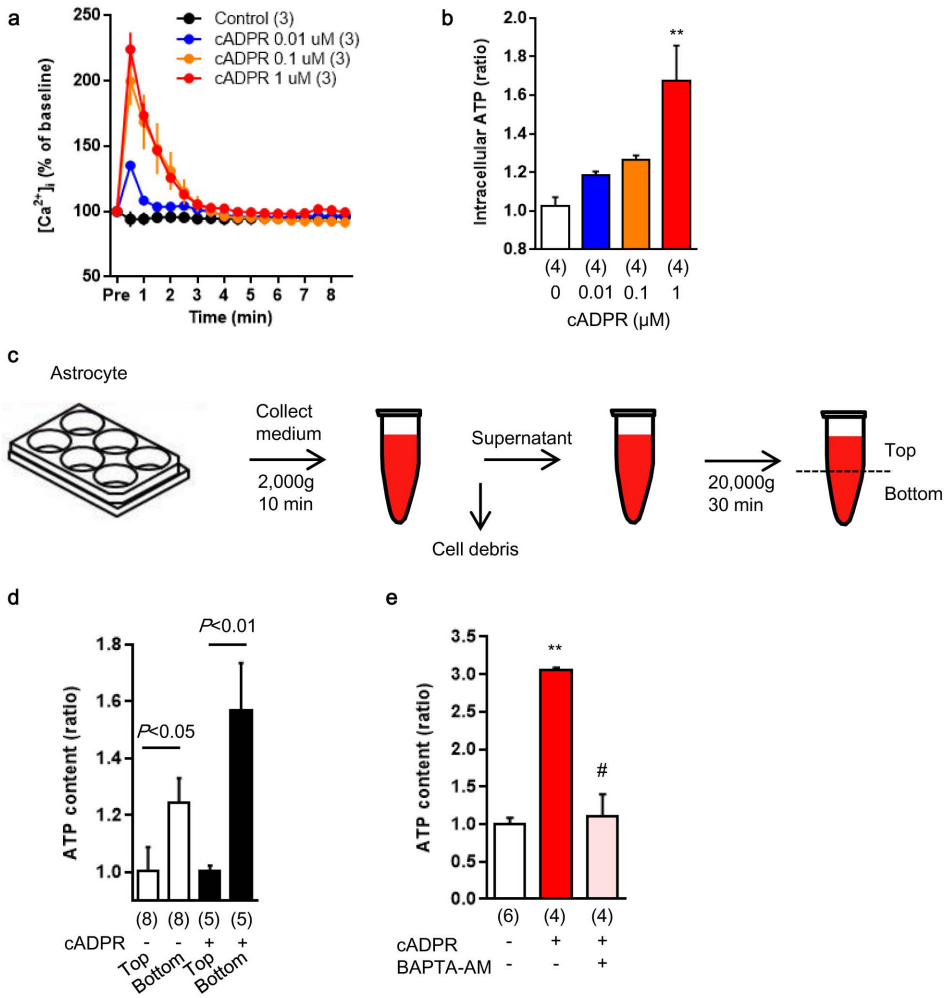

Extended Data Figure 3 | Production of astrocytic mitochondrial particles in a Ca^{2+}-dependent mechanism. a, The known CD38 downstream signal, cADPR, increased intracellular calcium levels shown by Fluo-4 intensity in a concentration-dependent manner ($n = 3$ independent experiments). **b**, Intracellular ATP levels in astrocytes were upregulated by cADPR stimulation ($n = 4$ independent experiments). $^{**}P < 0.01$ versus 0 μM cADPR. **c**, To measure ATP levels in extracellular particles, ACM was collected and large debris was excluded by centrifugation and filtration through a 1.2-μm filter. After another centrifugation at 20,000*g* for 30 min, 100 μl from the top or bottom fractions were used for the ATP assay. **d**, The bottom fraction had a higher ATP content, and cADPR (1 μM) increased the ATP content in this fraction ($n = 2$ biological replicates, $n = 8$ or 5 independent experiments). **e**, cADPR-induced extracellular ATP levels within extracellular particles were diminished by the intracellular calcium blocker, BAPTA-AM ($n = 2$ biological replicates, $n = 6$ or 4 independent experiments). Data are mean ± s.e.m. *P* values are from a one-way ANOVA followed by Tukey's test.

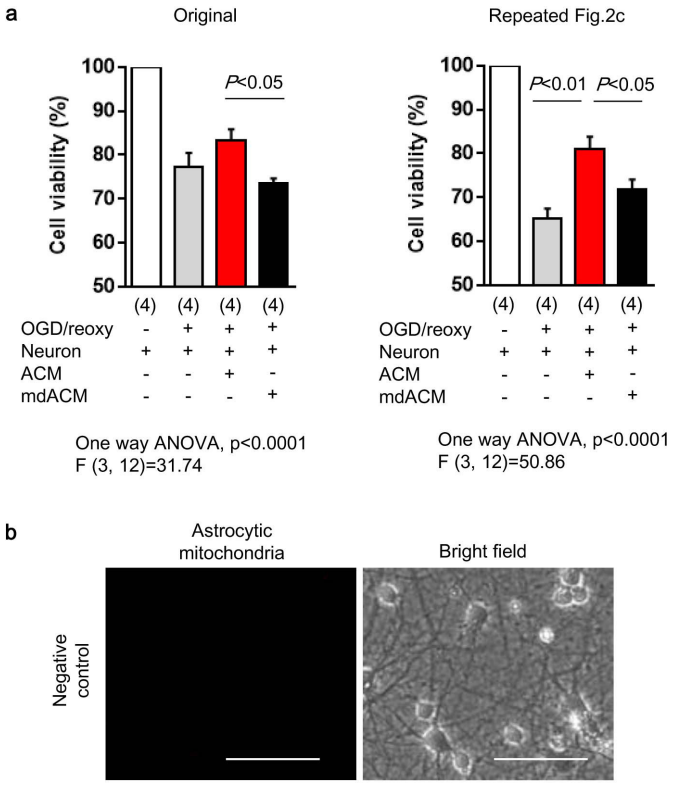

Extended Data Figure 4 | Summary of experiment in Fig. 2c. **a**, We repeated the experiment in Fig. 2c with $n = 4$ independent primary cultures per group. Similar results were obtained ($n = 2$ biological replicates, $n = 4$ independent experiments). The extracellular mdACM group was significantly different compared to the ACM group. Furthermore, in this repeated experiment, there was also statistical significance between controls (OGD-damaged neurons alone) versus those treated with mitochondria-containing astrocyte media (ACM), and there was no statistically significant worsening when comparing control versus mitochondria-depleted groups (mdACM). Taken together, these two separate experiments suggest a modest but statistically significant neuroprotection induced by astrocyte-derived mitochondria. Data are mean ± s.e.m. one-way ANOVA followed by Tukey's test. **b**, MitoTracker Red CMXRos (200 nM) was incubated without astrocytes to obtain no-cell-derived media (negative control). Media was collected and further incubated with neurons after OGD. After 24 h, there was no mitochondrial signal observed. Scale bars, 100 μm.

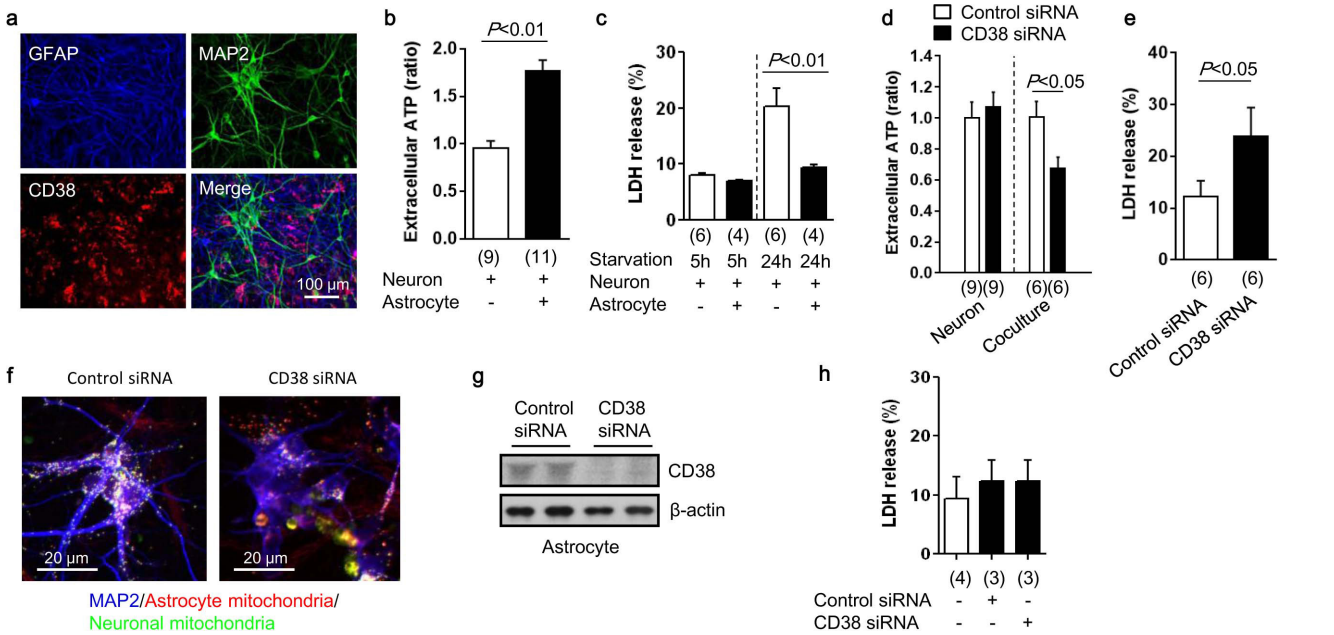

Extended Data Figure 5 | Role of astrocytic CD38 in mitochondria transfer during starvation *in vitro*. **a**, Immunocytochemistry in neuron–astrocyte co-cultures demonstrated that CD38 was primarily expressed within astrocytes. **b**, Extracellular ATP levels were higher in media collected from neurons co-cultured with astrocytes compared to media from neuron-alone cultures ($n = 3$ biological replicates, $n = 9$ or 11 independent experiments). **c**, After serum/glucose starvation, neurons were significantly damaged, as expected. But neurons co-cultured with astrocytes were protected ($n = 2$ biological replicates, $n = 6$ or 4 independent experiments). **d**, CD38 suppression by siRNA significantly decreased extracellular ATP levels in neuron–astrocyte co-cultures, but CD38 suppression did not affect extracellular ATP levels in neuron-alone cultures ($n = 3$ biological replicates, $n = 9$ or 6 independent experiments). **e**, Blockade of astrocytic CD38 by siRNA significantly increased LDH release (indicative of cell damage) in the co-cultures, suggesting that CD38 may be important for maintaining neuroglial homeostasis ($n = 2$ biological replicates, $n = 6$ independent experiments). **f**, Rat primary neurons were co-cultured with rat astrocytes. Immunocytochemistry showed that CD38 suppression by siRNA reduced astrocytic mitochondria (red) transfer into neurons compared to control. **g**, **h**, Western blot analysis indicated that CD38 suppression by siRNA can be successfully performed in astrocyte culture without affecting cell viability ($n = 2$ biological replicates, $n = 4$ or 3 independent experiments). Data are mean ± s.e.m. *P* values are from an unpaired *t*-test.

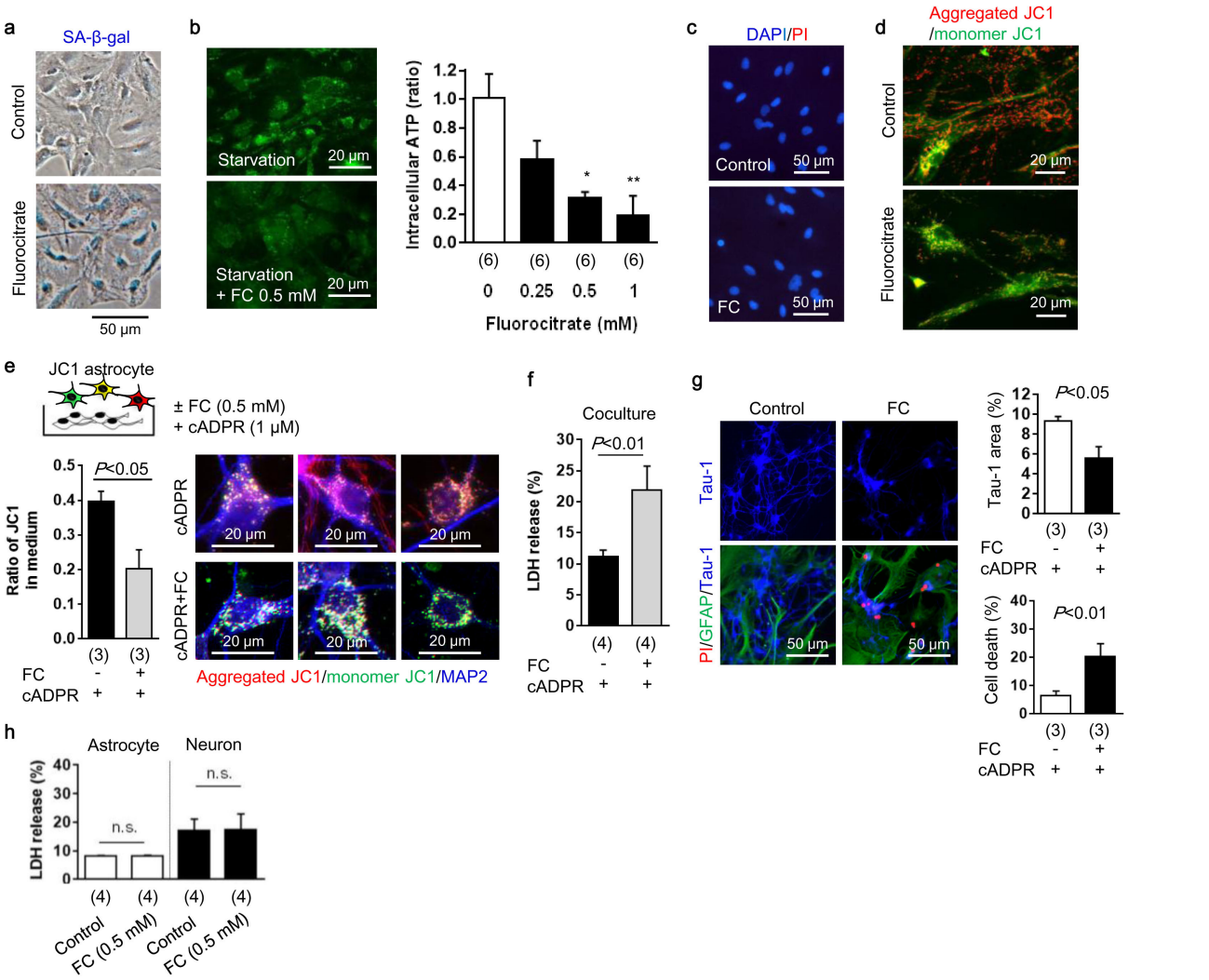

Extended Data Figure 6 | Metabolic inhibition in astrocyte causes neuronal cell death and prevents neurite outgrowth *in vitro*. **a**, Astrocytic aconitase was inhibited by fluorocitrate (FC), which disrupted astrocyte metabolism that was accompanied by a senescence-associated β-galactosidase (SA-β-gal) signal. **b**, Intracellular ATP was decreased in these metabolically disrupted astrocytes ($n = 2$ biological replicates, $n = 6$ independent experiments). $^{*}P < 0.05$, $^{**}P < 0.01$ versus 0 mM fluorocitrate. **c**, Propidium iodide (PI) staining showed that fluorocitrate (0.5 mM) did not induce cell death in astrocytes. **d**, Metabolically disrupted astrocytes significantly decreased the mitochondrial membrane potential. Red: aggregated JC1; green: monomer JC1. Scale bar, 20 μm. **e**, Rat cortical neurons were co-cultured with JC1-labelled astrocytes. After 24 h co-culture, control astrocytes transferred mitochondria, which had a high-membrane potential (aggregated JC1), but metabolically disrupted astrocytes released and transferred dysfunctional mitochondria into neurons ($n = 3$ independent experiments). **f**, Metabolically disrupted astrocytes could not support neural viability under starvation in the co-culture ($n = 4$ independent experiments). **g**, Co-culture between astrocytes and neurons was conducted for 48 h to test neurite outgrowth. Immunocytochemistry showed that metabolically disrupted astrocytes prevented neurite outgrowth and increased neuronal cell death ($n = 3$ independent experiments). **h**, The LDH assay indicated that fluorocitrate (0.5 mM) did not affect cell viability in either rat cortical astrocytes ($n = 4$ independent experiments) or rat cortical neurons ($n = 4$ independent experiments). Data are mean ± s.e.m. *P* values are from a one-way ANOVA followed by Tukey's test (**b**) or an un unpaired *t*-test (**e**–**g**).

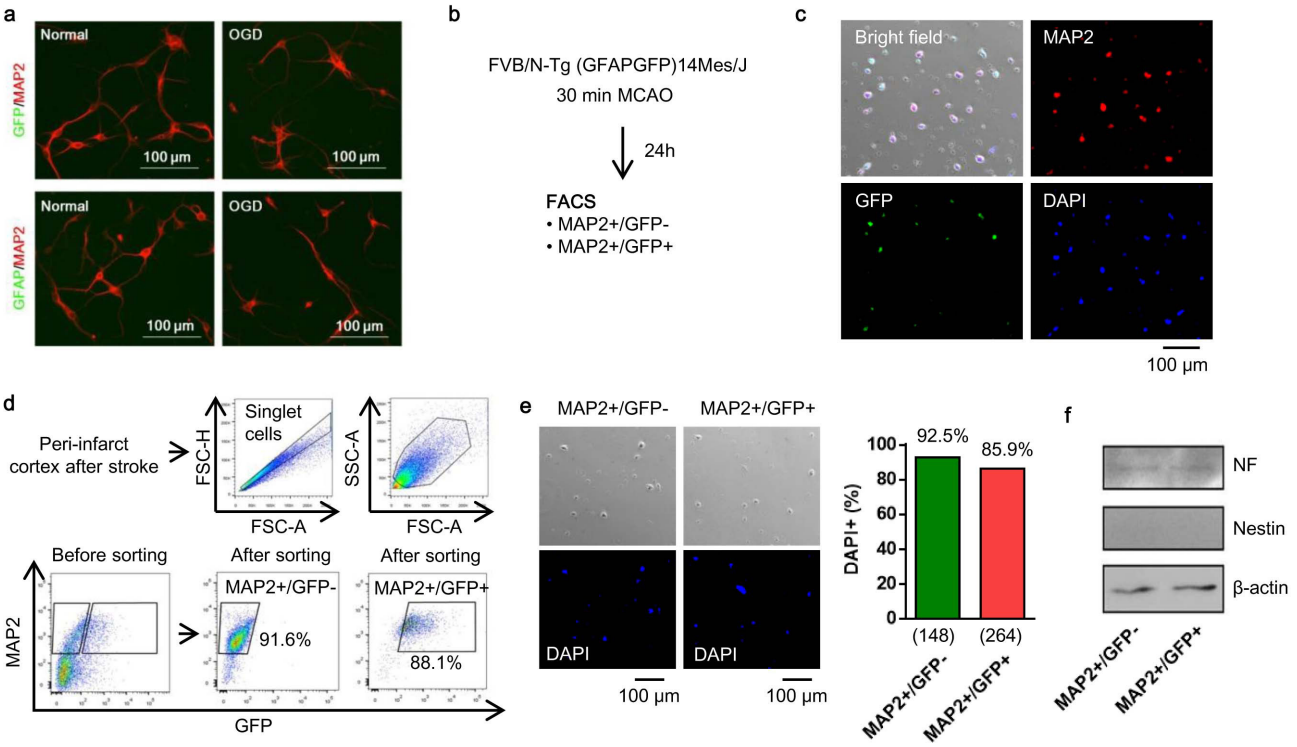

Extended Data Figure 7 | FACS analysis using E17 FVB/N-Tg (GFAPGFP)14Mes/J transgenic mice. a, Cortical neurons were isolated from E17 FVB/N-Tg (GFAPGFP)14Mes/J transgenic mice. Immunocytochemistry showed that cultured neurons did not express either GFP or GFAP protein after OGD, suggesting that stroke-like stress may not lead to 'leakiness' in this astrocyte-specific GFP mouse. **b**, Brain cell suspension was prepared from FVB/N-Tg (GFAPGFP)14Mes/J mice subjected to transient ischaemia, then FACS analysis was performed. **c**, Representative image before cell sorting. **d**, Purity after cell sorting. **e**, The $MAP2^{+}$ GFP^{-} or $MAP2^{+}$ GFP^{+} populations were 92.5% or 85.9% positive for DAPI, respectively. **f**, Western blot analysis demonstrated that both GFP-positive and -negative neurons expressed mature neuron marker (neurofilament) but not neuronal stem-cell marker (nestin). These data exclude the possibility that GFAP-positive cells included subsets of neuronal precursor cells that are known to also express GFAP.

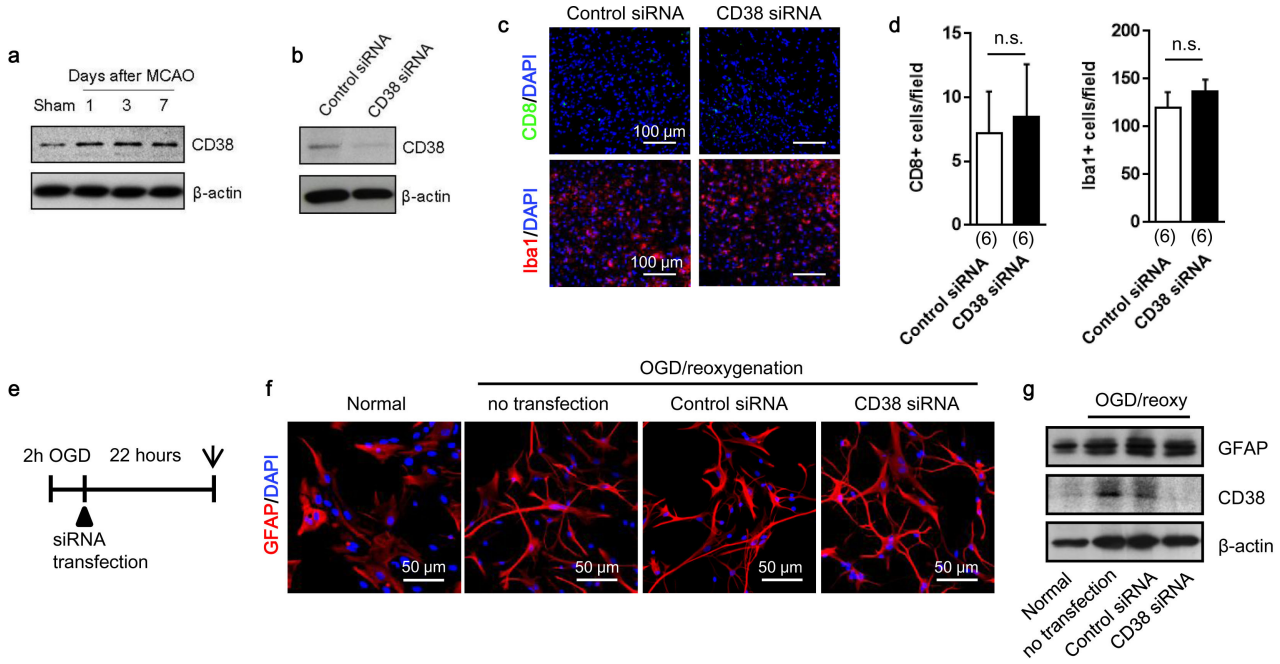

Extended Data Figure 8 | Effects of CD38 suppression by siRNA *in vivo* and *in vitro*. **a**, Western blot showed that CD38 expression was increased in peri-infarct cortex at days 1 to 7 after stroke. **b**, *Cd38* siRNA or a scrambled control was injected into lateral ventricles at 5 days after stroke. Western blot analysis confirmed that CD38 expression was successfully decreased in peri-infarct cortex at 7 days. **c**, In peri-infarct cortex, CD8 T-cell and Iba1-positive microglia/macrophages were detected by immunohistochemistry. **d**, Quantification of the number of CD8-positive or Iba1-positive cells indicated that there was no difference between control siRNA or *Cd38* siRNA ($n = 6$ mice per group). Data are mean ± s.e.m. **e**, Cultured rat cortical astrocytes were subjected to OGD for 2 h followed by treating with control siRNA or *Cd38* siRNA. Astrocyte cell morphology or GFAP expression was assessed by immunocytochemistry or western blot after 22 h reoxygenation. **f**, Morphology change was not clearly observed in cultured astrocytes treated with *Cd38* siRNA compared to control siRNA. **g**, Western blot analysis showed that CD38 was successfully decreased by siRNA transfection but GFAP expression was not changed.

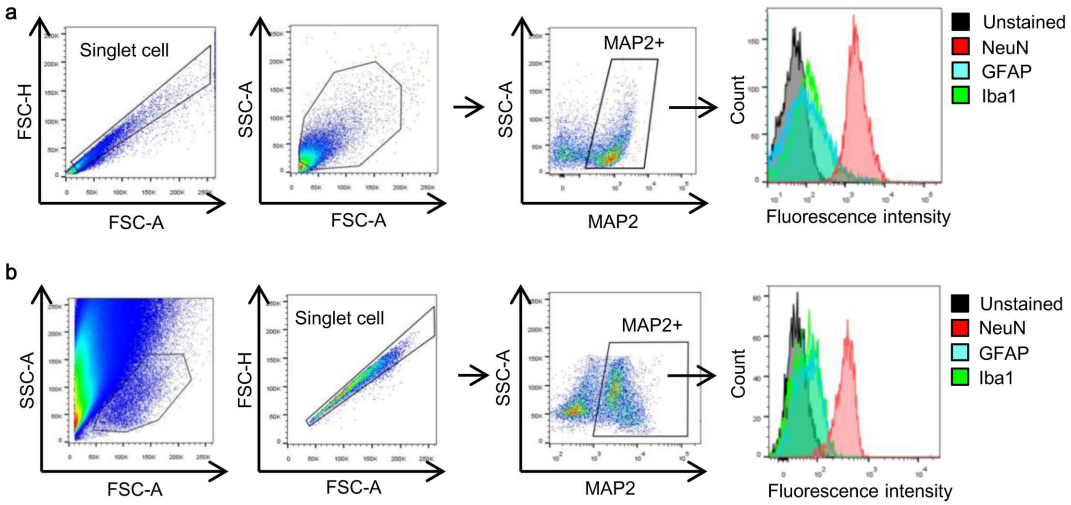

Extended Data Figure 9 | Neuronal purity confirmed by FACS analysis *in vivo*. To confirm our FACS findings, we used two different published standard approaches[32,33]. **a**, By FACS, the MAP2-positive population was gated and further assessed by markers such as Iba1 (microglia/macrophage) and GFAP (astrocyte) in brain cell samples isolated from C57BL/6 J mice. These comparisons confirmed that the MAP2^{+} population did not contain any appreciable amounts of microglia or astrocytes, whereas another neuron marker (NeuN) was highly enriched. **b**, Similar findings were obtained using an alternative gating method to isolate neurons.

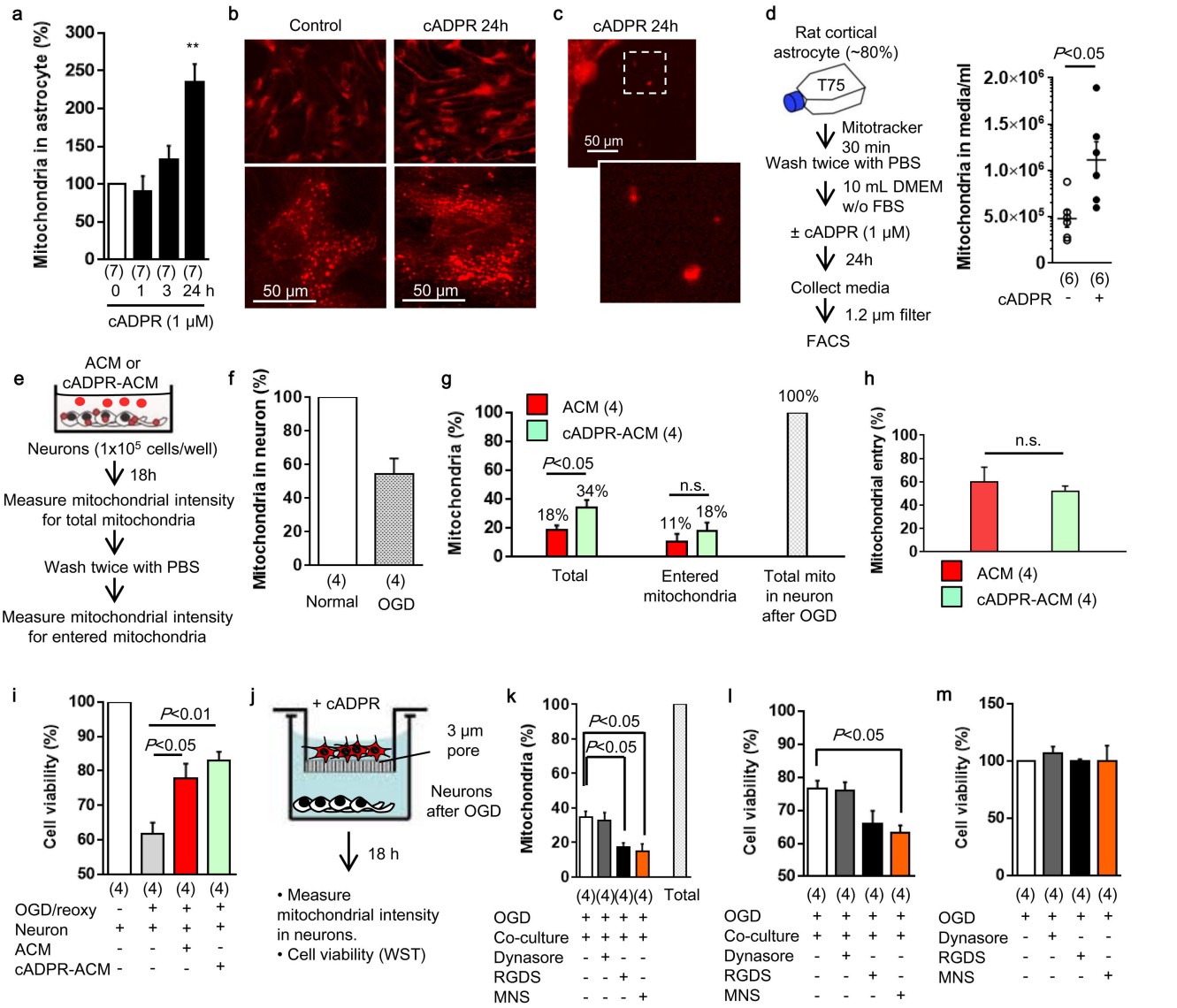

Extended Data Figure 10 | Involvement of integrin-mediated Src/Syk signalling mechanisms in astrocytic mitochondrial entry into neurons *in vitro*. **a**, **b**, Cultured rat cortical astrocytes were stimulated by cADPR (1 μM) for 24 h. Intracellular mitochondria labelled by MitoTracker dye was significantly increased in astrocytes stimulated with cADPR (1 μM) ($n = 2$ biological replicates, $n = 7$ independent experiments). $^{**}P < 0.01$ versus 0 h. **c**, Some mitochondria were found outside of cells. **d**, FACS analysis revealed that approximately 5×10^5 mitochondria were contained in 1 ml ACM. cADPR (1 μM) significantly increased the number of mitochondria in the media ($n = 2$ biological replicates, $n = 6$ independent experiments). **e**, Experimental schedule to quantify the entry of mitochondria into neurons after OGD. Rat cortical neurons (1×10^5 cells per well) were prepared in 24-well culture plates. ACM or cADPR-ACM (each 1 ml) was co-incubated with neurons for 18 h. Mitochondrial entry into neurons was calculated by mitochondrial intensity measured before and after washing cells with PBS. Phenol-red-free culture media was used to decrease the background signal. The background signal was subtracted from the fluorescent intensity obtained from each sample. **f**, OGD for 2 h decreased approximately 50% of the mitochondria in neurons after 18 h reoxygenation ($n = 2$ biological replicates, $n = 4$ independent experiments). **g**, Data are expressed as relative values, with total neuronal mitochondria after 2 h OGD/18 h reoxygenation being 100%. Mitochondrial entry into neurons was slightly higher after cADPR-ACM treatment (18%) compared to ACM treatment (11%), although there was no statistical significance ($n = 2$ biological replicates, $n = 4$ independent experiments). **h**, There was no difference in the percentage of mitochondrial entry after ACM treatment or cADPR-ACM treatment ($n = 2$ biological replicates, $n = 4$ independent experiments). **i**, cADPR-ACM treatment supported neuronal viability better than ACM treatment ($n = 2$ biological replicates, $n = 4$ independent experiments). **j**, Co-culture between rat cortical astrocytes in the upper chamber and rat cortical neurons in the lower chamber was performed for 18 h after OGD for 2 h in neurons. Mitochondrial entry into neurons was then measured. **k**, Immediately after OGD, dynasore (5 μM), RGDS peptide (H-Arg-Gly-Asp-Ser-OH; 50 μg ml^{-1}), or MNS (3,4-methylenedioxy-β-nitrostyrene; 1 μM) was initially added to neurons for 30 min, then astrocyte co-culture was performed for 18 h. Data are expressed as relative values, with astrocytic extracellular mitochondria plus entered mitochondria into neurons being 100%. RGDS peptide and MNS significantly decreased mitochondrial entry into neurons, but dynasore did not inhibit the entry. **l**, MNS treatment significantly decreased astrocyte-mediated neuroprotection ($n = 2$ biological replicates, $n = 4$ independent experiments). **m**, Dynasore (5 μM), RGDS peptide (50 μg ml^{-1}), or MNS (1 μM) did not affect neuronal viability after 2 h OGD ($n = 4$). Data are mean ± s.e.m. These data suggest that the entry of astrocytic mitochondrial particles into neurons may involve integrin-mediated Src/Syk signalling mechanisms. However, we acknowledge that these pathways may be multifactorial, and deeper analyses are warranted to dissect entry mechanisms under various physiological and pathological conditions. *P* values are from a one-way ANOVA followed by Tukey's test (**a, i, k, l**) or an unpaired *t*-test (**d, g**).

CORRECTIONS & AMENDMENTS

CORRIGENDUM

doi:10.1038/nature19805

Corrigendum: Transfer of mitochondria from astrocytes to neurons after stroke

Kazuhide Hayakawa, Elga Esposito, Xiaohua Wang, Yasukazu Terasaki, Yi Liu, Changhong Xing, Xunming Ji & Eng H. Lo

Nature **535,** 551–555 (2016); doi:10.1038/nature18928

In this Letter, in Fig. 1d and 1m, the *y* axis label should have read 'JC1 (red/green)' instead of 'JC1 (green/red)'; this has been corrected online.